International Journal on Interactive Design and Manufacturing (IJIDeM) (2018) 12:1007–1014
https://doi.org/10.1007/s12008-017-0433-9

ORIGINAL PAPER

Characterization of surface topography of 3D printed parts by multi-scale analysis

Yann Quinsat[1] · Claire Lartigue[1] · Christopher A. Brown[2] · Lamine Hattali[3]

Received: 28 October 2017 / Accepted: 22 November 2017 / Published online: 27 November 2017

Abstract
Surface topography is a key element between process parameters and manufactured part performances. Within the context of 3D printed parts, one difficulty is to consider the total 3D surface topography including internal porosity. In this paper, an original method is proposed for the characterization of the surface topography, both internal and external. Starting from volumetric data obtained by Computed Tomography measurements, a method of surface extraction is performed that identifies skin voxels corresponding to the internal and external part surface, and which are the support to the calculation of the Specific Surface Area (*SSA*). A multi-scale analysis is thus proposed to characterize the total surface, (*SSA*), obtained at different scales. The interest of the multi-scale analysis is illustrated through various examples that attempt to link process parameters to part properties.

Keywords 3-Dimensional printing · Computerized tomography · Multi-scale analysis · Specific surface area

1 Introduction

In additive manufacturing, the weight of parts can be optimized to support a given load by designing an internal structure [22], including porosity, using a given filling strategy. The structure, both internal and external, fully contributes to global mechanical properties of the produced part. As an example, periodic lattice structures, which consists of a unit cell regularly repeated in all directions, are designed and optimized to meet required level of mechanical, energetic, even acoustical performances [3,9,20,27] (Fig. 1). Although additive manufacturing allows the elaboration of more complex part geometries, the knowledge of the key control parameters is still unstructured, and as a result, geometrical variations during the production are poorly controlled. Given the large number of different geometries that can be elaborated using additive manufacturing, and without understanding of the influential parameters on geometrical variations, it seems essential to define simple indicators to facilitate interactivity in the design and manufacturing of these structures. Those indicators can assessed the process with regard the geometry produced. This is particularly important to pursue industrial development and take full advantage of additive manufacturing processes.

In this context, a challenging issue is to link process parameters to part performances (or properties), such as, for instance, mechanical properties. As the 3D surface topography results from process parameters, the approach classically adopted is to first establish relations between process parameters and 3D surface topography, before linking this topography to part performances (Fig. 2). Surface topography is thus considered as the key element between the manufacturing process and the part function. One difficulty for 3D printed parts is to take into account the total 3D surface topography, including internal porosity.

In this paper, we investigate the relation between the filling strategy and the resulting 3D surface topography, including internal topography, for 3D parts obtained by Fused Filament Fabrication (FFF). The aim of this study is to define parameters to characterize the surface topography and to discriminate various filling strategies. The proposed method relies on Computarized Tomography (CT) measurements, which allow the measurement of both the internal and the external topography. The originality of our approach lies in

✉ Yann Quinsat
yann.quinsat@ens-paris-saclay.fr

1 LURPA, ENS Cachan, Univ. Paris-Sud, Université Paris Saclay, 94235 Cachan, France

2 Surface Metrology Lab, WPI, Worcester, MA, USA

3 Fast Univ. Paris-Sud, Université Paris Saclay, 91405 Orsay, France

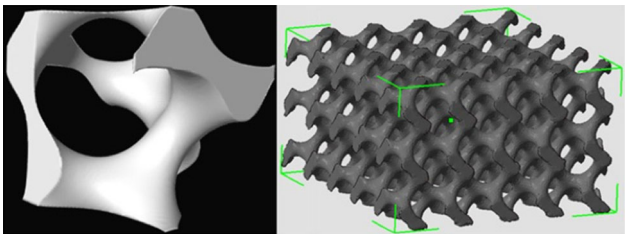

Fig. 1 A unit cell and associated periodic cellular lattice structure [27]

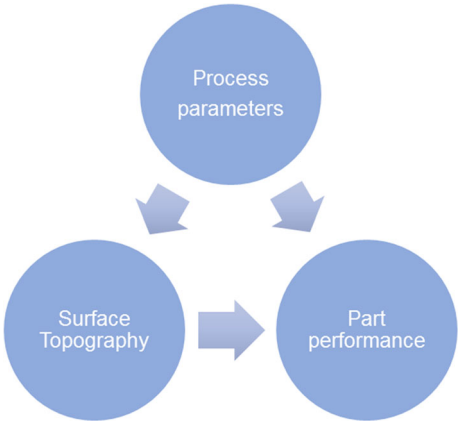

Fig. 2 Classic approach to link process parameters to surface properties

the use of multi-scale methods for analysis and characterization of the relative internal area calculated using the specific surface area. This paper is organized as follows. Section 2, is dedicated to related works. Section 3 details CT treatments we propose for Specific Surface Area calculation. In Sect. 4, the surface areas, including that of the pores, are characterized as a function of scale. Applications are proposed in Sect. 5.

2 Related works

The study of 3D surface topography obtained by FFF is a well-addressed question in the literature. The most classical approximation consists in modelling the external surface as a juxtaposition of elliptical pipes (or tubes) [1]. The influence of scanning and deposition directions on external topography during filling has been studied in [8,18]. Zeng et al. [28] show the influence of the process on local curvatures in a multi-scale analysis. An approach based on a finite element analysis is proposed in Jamiolahmadi and Barari [11] in order to predict 3D surface topography issued from FFF based on a few measured points. Meanwhile, Pupo et al. [19] establish the link between process parameters and the obtained topography in the case of sintering of metallic powders. Hence, most studies address the influence of process parameters on

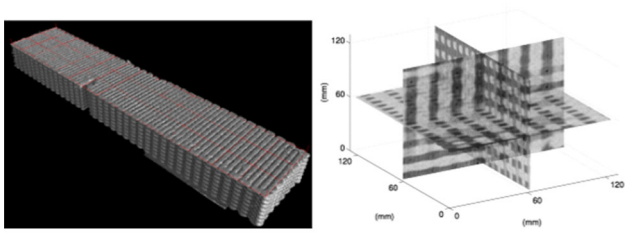

Fig. 3 Measurement using CT. **a** Example of one measured part, **b** data representation

external surface topography, but few works have studied the effect of process parameters on porosity. One difficulty lies in measuring the internal part surface. Computer Tomography (CT) now allows non-destructive 3D measurements of internal and external part geometry with uncertainties down to micrometers [2,6,25]. A recent study has shown the efficiency of CT in evaluating standard surface parameters to characterize 3D surface texture of metal additively manufactured parts [23]. Nevertheless, one of the main significant difficulties in CT measure treatments lies in the thresholding applied to the images in order to extract the part frontiers (or boundaries) [7]. Indeed, data issued from tomography represent the different levels of X-ray attenuation of the part for each point of the measured volume. The information is stored as a numerical value (gray level) in a volume element called a voxel [26]. Surface extraction from these 3D data (also referred to as 3D edge detection) is the first necessary stage for metrology applications [7,14], and is strongly linked to the voxel size which represents the tomography resolution [13]. As a result, CT measurement gives an estimate of the part geometry depending on the tomography resolution [13]. Some studies show that uncertainty in surface extraction can be reduced by making use of a sub-voxel resolution method which numerically improves CT resolution [14,26]. Uncertainty can achieve 1/10 of the voxel size when sub-voxel resolution is used [5], which makes CT applicable for dimensional metrology.

3 Surface extraction and Specific Surface Area calculation

From printed part (using Ultimaker 2 3-D printer), CT measurements were made which deliver information as a set of volumic data (voxels). A gray level is associated to each voxel in function of the absorbed amount of X-ray. CT measurements are thus represented as a set of volumic data link to material X-ray absorption, and can be displayed as a stock of images corresponding to different slices in one direction (Fig. 3).

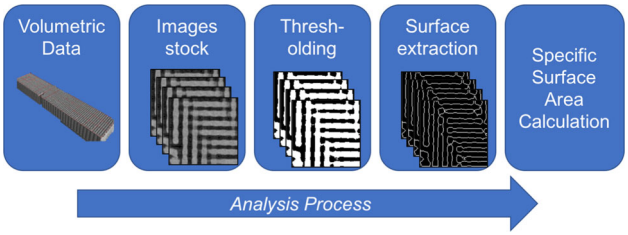

Fig. 4 Proposed method description

To conduct surface characterization, an automatic CT data treatment method is required. For metrology applications, the part geometry is defined from the contours of its surface (both external and internal). The main steps of the proposed method are displayed in Fig. 4. One main difficulty in using CT measurements, is the contour surface extraction from volumetric data. Ontiveros et al. [16] review surface extraction methods for metrology applications from CT. Among all the methods, threshold methods are commonly used for industrial applications: a gray level value is defined as a limit to differentiate the air and the material [16]. After image thresholding, surface contour extraction is performed, and calculation of parameters becomes possible. The next sections detail the different steps of our method.

3.1 Surface extraction

A threshold method, close to the algorithm proposed in [21] and using the Matlab Image Processing Toolbox, has been developed. The first step is image binarizing according to a threshold value determined with the well-known Otsus method [17]. Otsu's thresholding chooses the threshold to minimize the intraclass variance of the thresholded black and white pixels. This step is followed by a morphological operation on the binary image which removes interior pixels and keeps the outline of the shapes. Because surface extraction is the key point of surface characterization, and the basis for the evaluation of metrological quantities, our method was assessed as described below. For this assessment, a gauge block made in ZrO_2 is measured. This gauge ensures a flatness defect of 0.10 µm and a parallelism defect between its two faces of 0.10 µm. The calibrated distance between the 2 faces is 1.3 mm with an uncertainty of ± 0.12 µm at 20 °C. CT measurements are performed with a North Star Imaging (X50+) for which the voxel size is 5.9 µm × 5.9 µm × 5.9 µm. Finally, the measured volume consists of 200 × 300 × 1132 voxels. Our extraction method is applied leading to 2 sets of points, i.e., surface positions, each one corresponding to one of the 2 gauge faces (Fig. 5). To test the sub-voxel technique, the extraction method is applied considering a voxel-size that is 30% of the original one. This is simply obtained by a sub-voxel linear interpolation (Table 1).

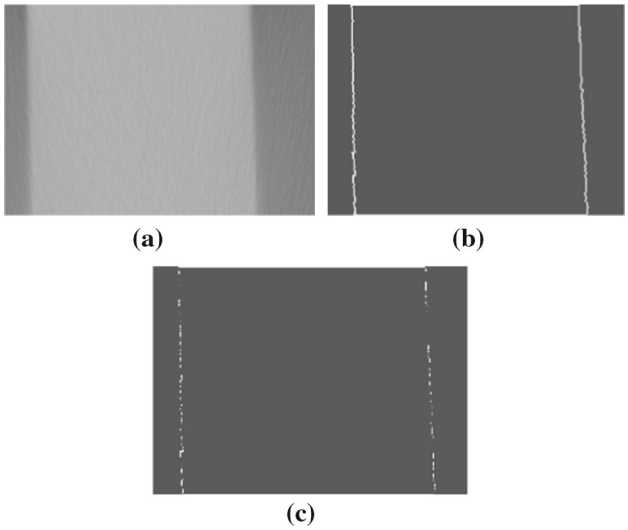

Fig. 5 Contour extraction for the gauge block. **a** Gauge measurement, **b** contour extraction (original voxel-size), **c** contour extraction (30% of the original voxel- size)

Table 1 Assessment of the surface extraction method

Voxel-size	Noise face 1 (µm)	Noise face 2 (µm)	Trueness
Original size	3	3.3	25.5
30% of original size	2.4	2.7	21.2

Assessment of the sub-voxel extraction considers two quality indicators, as proposed previously [15]: noise and trueness. Noise accounts for the measurement dispersion around each extracted face (a plane in practice), and trueness measures the difference between the calibrated distance and the measured distance obtained after face extraction (plane-plane distance). Results, displayed in Table 2, are consistent with the gauge quality, which illustrates the efficiency of our surface extraction method. It also can be observed that the noise along with the trueness is decreased when using a smaller voxel-size. This interesting result shows that sub-voxel refinement, as suggested by numerous studies [12,16,26] actually improves surface extraction.

3.2 Specific Surface Area (*SSA*) calculation

The Specific Surface Area (*SSA*) can be defined from the boundaries of the skeleton defined in 3D, which comprises the internal structure of the part. The boundaries are both internal to the part and on the exterior of the part. To simplify the representation, an example of the skeleton's construction in a 2D cross section is shown in Fig. 6.

According to voxel-map, the surface extraction leads to the identification of all the *skin* voxels, V_{skin}, which contain a portion of the skeleton skin (i.e., internal or external surface

Table 2 Design of experiment using L9 table ("Appendix A")

Factor	Level 1	Level 2	Level 3
Thickness (mm)	0.15	0.2	0.25
Directions (°)	0/90	30/120	45/135
Filling rate (%)	60	80	100

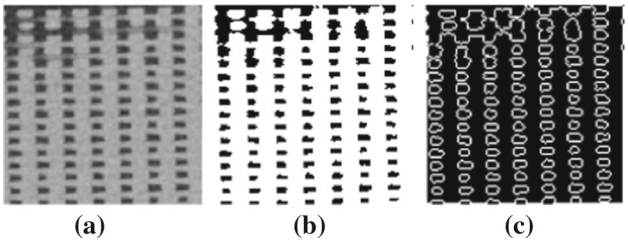

Fig. 6 Surface extraction from the skeleton in a cross-section. **a** Measurement, **b** binarized image, **c** skeleton skin

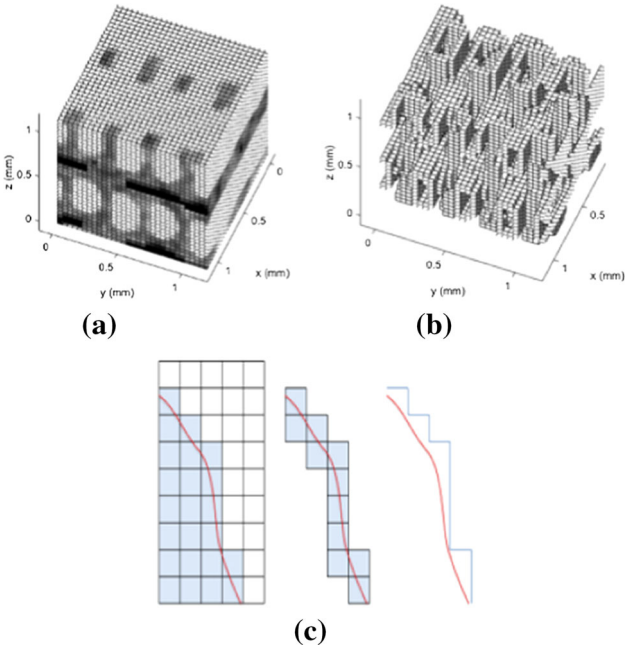

Fig. 7 Voxel representation of surface extraction. **a** Original voxel map, **b** skin voxel representation, **c** skin voxel extraction

of the structure) (Fig. 7b). The internal area is first calculated as the sum of all the areas of the skin voxel faces:

$$A = \sum_{i=1}^{V_{skin}} \sum_{j=1}^{6} A_{i,j}.\delta_{i,j} \tag{1}$$

where $A_{i,j}$ is the area of the face j belonging to the voxel i, and with:

$$\begin{cases} \delta_{i,j} = 1, \textit{ the face } j \textit{ belonging to the voxel } i \\ \qquad\quad \textit{is in contact with the air} \\ \delta_{i,j} = 0, \textit{ the face } j \textit{ belonging to the voxel } i \\ \qquad\quad \textit{is } \textbf{not} \textit{ in contact with the air} \end{cases} \tag{2}$$

Considering a 2D representation of a specimen measurement, the set of skin voxels corresponds to the blue voxels in the center of Fig. 7c. A profile of the calculated area A is shown by the red line to the right of Fig. 7c. The calculated area depends on the overall size of the region being analyzed. Specific surface area (*SSA*) is defined as the total surface area of a material per unit of volume (units of m^2/m^3 or m^{-1}). It has a particular importance for permeability, adsorption and reaction on surfaces. To obtain the Specific Surface Area (*SSA*), A is divided by the volume of the original voxel-map being analyzed, V_{tot} (Fig. 7a):

$$SSA = \frac{A}{V_{tot}} \tag{3}$$

4 Total surface characterization by multi-scale analysis

In order to conduct a multi-scale geometric analysis, such as have been applied to measured topographies for length, area, filling and curvature [4,24], *SSA* must be characterized as a function of scale. The assumed voxel size (AVS) in this case defines the scale for calculating *SSA*, and can be considered as the image resolution. The value of the AVS can have scales smaller (sub-voxel) and larger (meta-voxel) than the measured voxel size (MVS). This scale variation is equivalent to varying the length of the step in length-scale analysis for instance [4]. For the considered AVS, the material density belonging to a voxel is calculated by a linear interpolation from the MVS. As illustrated in Fig. 9 this strongly influences surface extraction. The corresponding parameter *SSA* is thus calculated. The parameter *SSA*, calculated as a function of scale, evolves, increasing somewhat linearly with a decreasing logarithmic scale to a plateau (Fig. 8). The original voxel sizes are 37.8 µm × 37.8 µm × 37.8 µm, and the bounding voxel size is set to 5 mm × 5 mm × 5 mm. The plateau begins around the scale of the original measured voxel ($MVS = 0.5410^{-4}$ mm^3, indicated by the vertical blue dashed-line in the picture). This indicates that the numerical sub-voxel treatment (inferior scales) does not provide additional information about the specific area. On the other hand, meta-voxels give information too far from reality. When AVS is close to 0.6 mm^3, surface extraction is not correct, and the value of *SSA* is not realistic. The study can thus be restricted to the zone for which AVS is less than 0.06 mm^3.

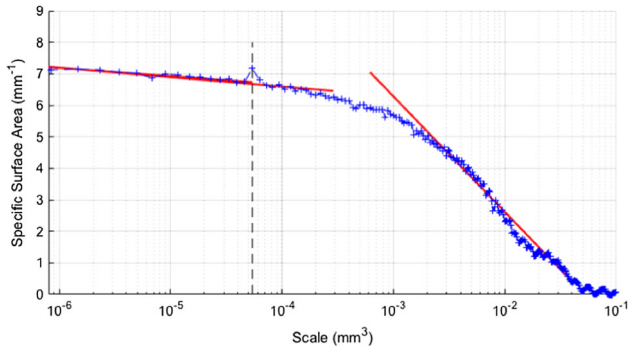

Fig. 8 Evolution of *SSA* as a function of the scale

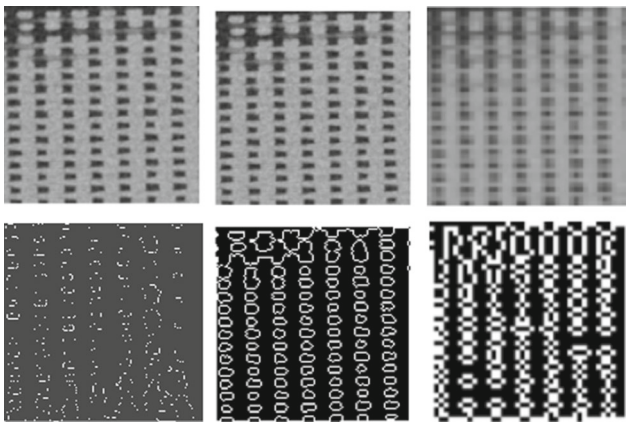

Fig. 9 Surface extraction as a function of scale *from left to right (top)*: measurement at scale 0.3, scale 1, and scale 3, *from left to right (bottom)*: surface extraction at scale 0.3, scale 1 and scale 3

5 Applications and discussion

The interest of the multi-scale characterization is illustrated through three applications. The first one in an attempt to link 3D surface topography and mechanical properties according to process parameters. The second application addresses the influence of process parameters on resulting printed surfaces, and the third one concerns the use of such a method to discriminate the different patterns obtained when using different filling strategies.

5.1 Critical stress intensity fracture K_C

The first study focuses on the influence of FFF (Fused Filament Fabrication) process parameters on fracture properties of the manufactured parts. Within the context of fracture studies, a series of bending specimens has been manufactured by varying the process parameters with the pattern geometry resulting from the zig-zag mode. Process parameters are thickness, filling directions and filling rate (see Table 2). Taguchis statistical design of experiment (DOE) technique was applied according to a table L9 orthogonal array with three factors for three levels (see Table 4 in "Appendix A").

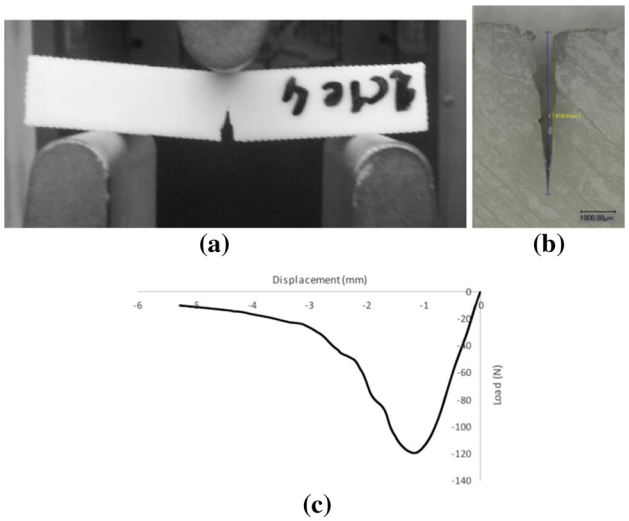

Fig. 10 Description of the cracking tests. **a** 3-Point bending setup, **b** crack initiation, **c** typical load evolution versus displacement

All the specimens were made with a small notch (Fig. 10a). The crack was made by pushing a wedge (razor blade) into the notch, quasi-statically, under controlled slowly increasing force, using a tensile machine. Following crack initiation, a 3-point bending test was performed to determine K_C, the critical stress intensity factor corresponding to fracture initiation. Although the presented work focuses on porous materials, the classical definition of K_C from the obtained curves (Fig. 10c) is used (ISO 13586 [10]). The results displayed in Table 1 clearly highlight the strong influence of the process parameters on the value of Kc. Therefore, knowledge of the relations between strength and filling strategies is necessary for product and process design optimization.

In our analysis, we attempt to link the resulting surface topography via *SSA* to K_C, the critical stress intensity factor. As observed in Fig. 11, there is no correlation between K_C and *SSA*, whatever the scale of observation. K_C does not appear to be relevant to link the function with the surface topography.

5.2 Study of process parameters

The second illustration aims at studying the influence of process parameters on the printed surface. The 9 manufactured specimens are measured using CT, and a multi-scale analysis of the *SSA* is conducted, yielding the results displayed in Fig. 12.

For low scales (i.e. sub-voxel scales), some specimens seem to reach the same value of *SSA* (specimens 1 and 6, and specimens 3 and 5). All the values are reported for sub-voxel scales, although, as previously mentioned, scales under 10^{-5} mm^3 do not give additional information. The study could be limited to scales lesser than 3 times the original

Table 3 Values of Kc (from design of experiment defined in Table 3)

Tests	1	2	3	4	5	6	7	8	9
Kc (MPa $\sqrt{m}$)	0.54	1.27	1.68	0.99	2.03	0.78	0.55	0.68	0.61

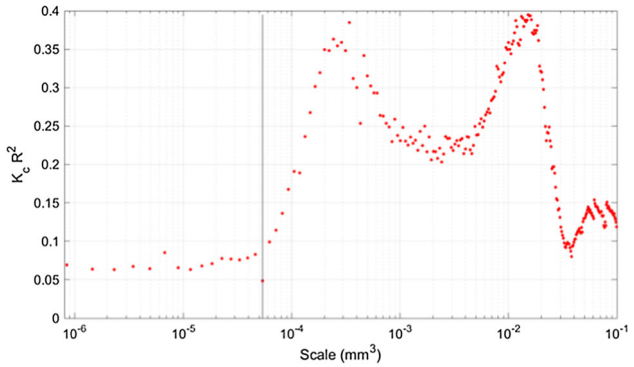

Fig. 11 Multi-scale analysis of the correlation of K_C with *SSA*

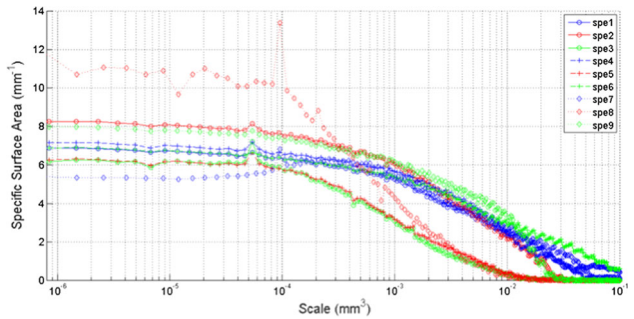

Fig. 12 Multi-scale analysis associated to the design of experiment

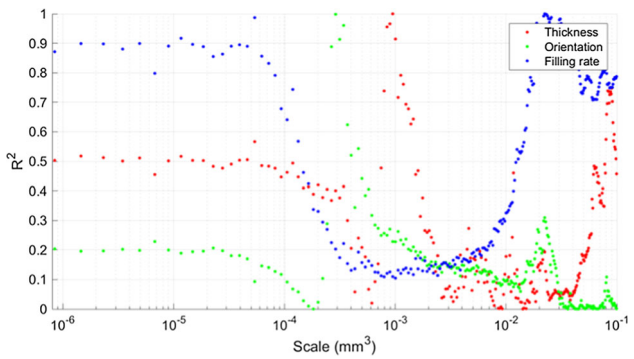

Fig. 13 Multi-scale analysis of the correlation factor with *SSA*

measured voxel. The evolution is different in the zone in which the *SSA* linearly increases with the decrease of scales. Indeed, the slope varies for each specimen, which should enable process parameter discrimination. The three parameters have different effects on *SSA*.

Correlation depends on the scale (Fig. 13). It tends to 1 for the filling rate at the scale of the original measured voxels, whereas the correlation value reaches 1 for greater scales

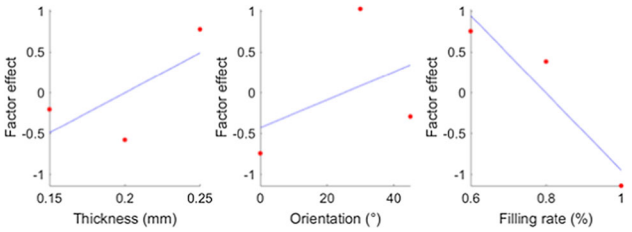

Fig. 14 Factor main effects at the original scale

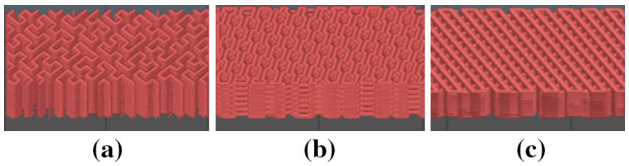

Fig. 15 The 3 different filling strategies. **a** Hilbert curve, **b** Honey curve, **c** ZigZag curve

for the thickness ($scale = 3.10^{-4}$ mm^3) and orientation ($scale = 10^{-3}$ mm^3).

Effects analyzed at the original scale (Fig. 14) show the significant linear effect of the filling rate parameter on *SSA*. The factor effect linearly decreases with the increase of the filling rate. This is not surprising, as porosity is strongly linked to the percentage of the filling rate. Other process parameters also present an effect on *SSA*, but it is more difficult to interpret.

5.3 Pattern geometry discrimination

For this application, the three different filling modes, giving three different pattern geometries described in Fig. 15, are tested with the same process parameters: thickness is set to 0.25 mm, and the filling percentage is set to 60%. The multi-scale analysis is applied to the CT measurement obtained for the 3 specimens. Results show that the evolution of *SSA* differs depending on the pattern geometry (Fig. 16). This is particularly distinct at low scales for which the greater value of *SSA* is obtained for the zig-zag strategy. The linear decrease with the increase of the scale is in turn lower for the Honey strategy. The Hilbert strategy presents the least variation of *SSA* for the whole range of scales. It worth noting, that a numerical effect in image resizing generates some outliers at a scale close to the original scale. But this does not affect the analysis. Actually, Multi-scale analysis of the *SSA* parameter enables 3D printed surface characterization, and appears as though it could be useful for filling strategy discrimination.

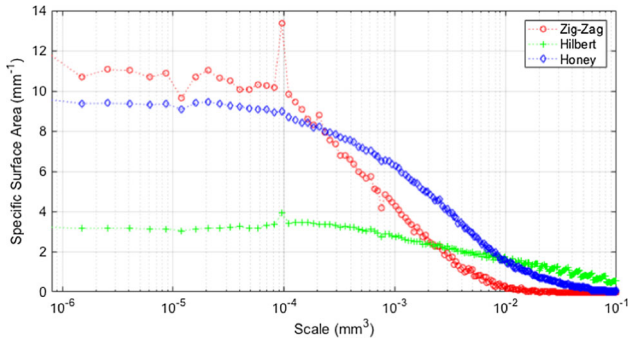

Fig. 16 Pattern geometry comparison using multi-scale analysis

6 Conclusion

Within the context of part manufacturing, it is essential to be able to link process parameters with the part function. This is particularly important for lattice structures obtained in additive manufacturing, as both internal and external surface topographies fully contribute to the global mechanical properties of the produced part. These surface topographies result from the filling strategy. Therefore, the link between the process parameters and the function can be established by characterizing both the internal and external surface topography. In our study, based on CT measurements, we introduce the *SSA*, the Specific Surface Area, which is used to analyze the relative internal area of the total surface, including that of pores. The set of skin voxels defined the 3D surface topography, both internal and external. To link process parameters to the manufactured surface, a multi-scale discrimination method is proposed: *SSA* is characterized as a function of scale. To show the relevance of multi-scale *SSA* analysis, two different applications are proposed. The first one clearly highlights the interest of our approach to discriminate filling modes when using FFF. For the second application, the filling mode is the same (zig-zag mode), and the study focuses on the influence of some process parameters (thickness, pattern geometry, and filling rate) on the printed surface. This study confirms the relevance of using *SSA* to discriminate surface topographies obtained with different process parameters. The analysis of the effects can be performed at different scales with the aim of finding out the most relevant scale of study. For instance, we show that the effect of the Filling rate is significant and linear at the original scale. Nevertheless, in this study no correlation is observed between K_C, the critical stress intensity factor, and *SSA*, whatever the scale of observation. The link between the function and process parameters cannot be established with this parameter. According to multiscale analysis, further work could focus on linking energy release rate and internal relative area.

Acknowledgements Authors would thank Zeiss Industrial Metrology, LLC which provides all the CT measurements.

Appendix A: Taguchi L_9

See Table 4.

Table 4 Table L_9

Specimen n°	Factor 1	Factor 2	Factor 3	Factor 4
1	1	1	1	1
2	1	2	2	2
3	1	3	3	3
4	2	1	2	3
5	2	2	3	1
6	2	3	1	2
7	3	1	3	2
8	3	2	1	3
9	3	3	2	1

References

1. Ahn, D., Kweon, J.H., Kwon, S., Song, J., Lee, S.: Representation of surface roughness in fused deposition modeling. J. Mater. Process. Technol. **209**(15–16), 5593–5600 (2009)
2. Bartscher, M., Hilpert, U., Goebbels, J., Weidemann, G.: Enhancement and proof of accuracy of industrial computed tomography (CT) measurements. CIRP Ann. Manuf. Technol. **56**(1), 495–498 (2007)
3. Beyer, C., Figueroa, D.: Design and analysis of lattice structures for additive manufacturing. ASME J. Manuf. Sci. Eng. **138**(12), 121014 (2016)
4. Brown, C.A., Johnsen, W.A., Hult, K.M.: Scale-sensitivity, fractal analysis and simulations. Int. J. Mach. Tools Manuf. **38**(5–6), 633–637 (1998)
5. Carmignato, S.: Accuracy of industrial computed tomography measurements: experimental results from an international comparison. CIRP Ann. Manuf. Technol. **61**(1), 491–494 (2012)
6. De Chiffre, L., Carmignato, S., Kruth, J.P., Schmitt, R., Weckenmann, A.: Industrial applications of computed tomography. CIRP Ann. Manuf. Technol. **63**(2), 655–677 (2014)
7. Dewulf, W., Kiekens, K., Tan, Y., Welkenhuyzen, F., Kruth, J.P.: Uncertainty determination and quantification for dimensional measurements with industrial computed tomography. CIRP Ann. Manuf. Technol. **62**(1), 535–538 (2013)
8. Galantucci, L., Lavecchia, F., Percoco, G.: Experimental study aiming to enhance the surface finish of fused deposition modeled parts. CIRP Ann. Manuf. Technol. **58**(1), 189–192 (2009)
9. Hussein, A., Hao, L., Yan, C., Everson, R., Young, P.: Advanced lattice support structures for metal additive manufacturing. J. Mater. Process. Technol. **213**, 1019–1026 (2013)
10. ISO 13586:2000 plastics determination of fracture toughness (GIC and KIC) linear elastic fracture mechanics (LEFM) approach (2000)
11. Jamiolahmadi, S., Barari, A.: Surface topography of additive manufacturing parts using a finite difference approach. J. Manuf. Sci. Eng. **136**(4), 18 (2014)
12. Jimnez, R., Comps, C., Yage, J.: An optimized segmentation algorithm for the surface extraction in computed tomography for metrology applications. Procedia Eng. **132**, 804–810 (2015)

13. Kruth, J., Bartscher, M., Carmignato, S., Schmitt, R., Chiffre, L.D., Weckenmann, A.: Computed tomography for dimensional metrology. CIRP Ann. Manuf. Technol. **60**(2), 821–842 (2011)
14. Lifton, J.J., Malcolm, A.A., McBride, J.W.: On the uncertainty of surface determination in X-ray computed tomography for dimensional metrology. Meas. Sci. Technol. **26**(3), 035003 (2015)
15. Mehdi-Souzani, C., Quinsat, Y., Lartigue, C., Bourdet, P.: A knowledge database of qualified digitizing systems for the selection of the best system according to the application. CIRP J. Manuf. Sci. Technol. **13**, 15–23 (2016)
16. Ontiveros, S., Yage, J., Jimnez, R., Brosed, F.: Computer tomography 3d edge detection comparative for metrology applications. Procedia Eng. **63**, 710–719 (2013)
17. Otsu, N.: A threshold selection method from gray-level histograms. IEEE Trans. Syst. Man Cybern. **9**(1), 6266 (1979)
18. Pandey, P.M., Reddy, N.V., Dhande, S.G.: Improvement of surface finish by staircase machining in fused deposition modeling. J. Mater. Process. Technol. **132**(1–3), 323–331 (2003)
19. Pupo, Y., Monroy, K.P., Ciurana, J.: Influence of process parameters on surface quality of CoCrMo produced by selective laser melting. Int. J. Adv. Manuf. Technol. **80**(5–8), 985995 (2015)
20. Rosen, D., Johnston, S., Reed, M., Wang, H.: Design of general lattice structures for lightweight and compliance applications. In: Rapid Manufacturing Conference, July 5–6 2006, Loughborough University (2006)
21. Shahabi, H., Ratnam, M.: Simulation and measurement of surface roughness via grey scale image of tool in finish turning. Precis. Eng. **43**, 146–153 (2016)
22. Thompson, M.K., Moroni, G., Vaneker, T., Fadel, G., Campbell, R.I., Gibson, I., Bernard, A., Schulz, J., Graf, P., Ahuja, B., Martina, F.: Design for additive manufacturing: trends, opportunities, considerations, and constraints. CIRP Ann. Manuf. Technol. **65**, 737760 (2016)
23. Townsend, A., Pagani, L., Scott, P., Blunt, L.: Areal surface texture data extraction from X-ray computed tomography reconstructions of metal additively manufactured parts. Precis. Eng. **48**, 254–264 (2017)
24. Vulliez, M., Gleason, M., Souto-Lebel, A., Quinsat, Y., Lartigue, C., Kordell, S., Lemoine, A., Brown, C.: Multi-scale curvature analysis and correlations with the fatigue limit on steel surfaces after milling. Procedia CIRP **13**, 308–313 (2014)
25. Wang, J., Leach, R.K., Jiang, X.: Review of the mathematical foundations of data fusion techniques in surface metrology. Surf. Topogr. Metrol. Prop. **3**(2), 023001 (2015)
26. Yage-Fabra, J., Ontiveros, S., Jimnez, R., Chitchian, S., Tosello, G., Carmignato, S.: A 3D edge detection technique for surface extraction in computed tomography for dimensional metrology applications. CIRP Ann. Manuf. Technol. **62**(1), 531–534 (2013)
27. Yan, C., Hao, L., Hussein, A., Raymont, D.: Evaluations of cellular lattice structures manufactured using selective laser melting. Int. J. Mach. Tools Manuf. **62**, 3238 (2012)
28. Zeng, Y., Wang, K., Wang, B., Brown, C.: Multi-scale evaluations of the roughness of surfaces made by additive manufacturing. In: ASPE—2014 Spring Topical Meeting (2014)